Proposal of a general scheme to obtain room-temperature spin polarization in asymmetric antiferromagnetic semiconductors

Xingxing Li,[1] Xiaojun Wu,[1,2,3] Zhenyu Li,[1] and Jinlong Yang[1,3,*]

[1]*Hefei National Laboratory for Physical Sciences at the Microscale, University of Science and Technology of China, Hefei, Anhui 230026, China*

[2]*Chinese Academy of Sciences Key Laboratory of Materials for Energy Conversion and Department of Materials Science and Engineering, University of Science and Technology of China, Hefei, Anhui 230026, China*

[3]*Synergetic Innovation Center of Quantum Information and Quantum Physics, University of Science and Technology of China, Hefei, Anhui 230026, China*

(Received 26 December 2014; revised manuscript received 2 July 2015; published 18 September 2015)

Exploring magnetic semiconductors is one of the most important questions for spintronic applications. Although various solutions, such as dilute magnetic semiconductors, have been proposed, a practical spintronic device working at room temperature has not been realized. The key to address this issue is to find magnetic materials with both room-temperature magnetic ordering and large spin polarization around the Fermi energy level. Here, we predict a new concept of asymmetric antiferromagnetic (AFM) semiconductors (AAFMSs) with both features. The high temperature magnetic ordering originates from the AFM coupling between different transition metal ions with strong super-exchange interaction, whereas the large spin polarization around the Fermi energy level owes to *d* orbital mismatch among these ions. Through first-principles calculations, a family of double perovskites A_2CrMO_6 (A = Ca,Sr,Ba, and M = Ru,Os) are predicted to be AAFMSs. This paper provides a way for developing spintronic devices working at room temperature.

DOI: 10.1103/PhysRevB.92.125202 PACS number(s): 71.15.Mb, 75.50.Pp

As candidate materials for spintronics, magnetic semiconductors have attracted many research interests, partly due to the great advantage of easy implementation in devices by utilizing nowadays well-developed semiconductor technology. According to the spin polarization at valence band maximum (VBM) and conduction band minimum (CBM), magnetic semiconductors can be divided into half semiconductors (HSCs) [1,2], spin gapless semiconductors (SGSs) [3,4], and bipolar magnetic semiconductors (BMSs) [5,6], etc.

To develop practicable spintronic devices with magnetic semiconductors, at least two essential issues should be considered. First, the magnetic ordering should survive at room temperature. Second, large spin polarization at VBM and CBM is required. To create magnetic semiconductors that work at room temperature was a topic raised in 2005 as one of 125 big questions in science [7]. However, after 10 years of exploration, this problem is still not well solved.

Up to now, magnetic semiconductors that meet the above two requirements are scarce [8,9], and we still lack a general scheme to achieve such materials. On one hand, large spin polarization at VBM and CBM can be easily obtained in ferromagnetic (FM) semiconductors, while their Curie temperatures are usually below the room temperature due to the fact that the FM super-exchange interaction is generally weak [10–12]. On the other hand, in antiferromagnetic (AFM) semiconductors, the Néel temperature is often high, whereas their VBM and CBM are spin nonpolarized [13,14].

To solve this inconsistency, a potential route is to develop diluted magnetic semiconductors (DMSs) by doping nonmagnetic semiconductors with small amounts of magnetic ions [15–19]. The basic mechanism is that the extrinsically doped carrier mediated FM exchange interactions between diluted magnetic ions can help induce a magnetic order probably up to room temperature [20]. Although several DMSs have been reported recently to show FM-like properties persisting over room temperature, the ferromagnetism therein actually resulted from nanoscale phase separations, which dramatically depend on the growth conditions and postgrowth processing. The demonstration of a device structure working at room temperature is still blank [21–23].

In this paper, we propose a picture of magnetic semiconductors, named as the asymmetric AFM semiconductors (AAFMSs), which simultaneously possess room-temperature magnetic ordering and large spin polarization at VBM and CBM. "Asymmetric" refers to different distributions of density of states (DOS) in spin-up and spin-down channels, despite the AFM nature of the material.

Asymmetric AFM semiconductors ingeniously combine the advantages of both FM and AFM semiconductors. This is the result of well-designed magnetic and electronic structures for AAFMSs. First, magnetic moments are designed to be carried by different transition-metal ions with AFM ordering and cancelled out by each other. The strong AFM super-exchange interaction ensures a high Néel temperature. Second, VBM and CBM are highly spin polarized as a result of *d* orbital mismatch among different transition-metal ions. The concept of AAFMSs is verified by the first-principles calculations on a series of double perovskites A_2CrMO_6 (A = Ca,Sr,Ba; M = Ru,Os), which have AFM orders above room temperature and exhibit diverse spin-polarization patterns. Among them, A_2CrRuO_6 are AFM HSCs with VBM and CBM fully spin polarized in the same direction, which is promising for spin-polarized carrier injection and detection. The A_2CrOsO_6 are AFM BMSs with VBM and CBM approaching the Fermi level through opposite spin channels, possessing great potential in electrical control of the carrier's spin orientation applications [11,12,24,25]. Further calculations confirm that

*jlyang@ustc.edu.cn

chemical doping of these semiconductors can induce either n- or p-type conductivity with a high spin polarization at the Fermi level.

During calculations, the structure and cell optimizations of A_2CrMO_6 are carried out within the Perdew-Burke-Ernzerhof generalized gradient approximation (GGA) [26] implemented in the Vienna *Ab initio* Simulation Package (VASP) [27]. The projector augmented wave (PAW) potential [28] and the plane-wave cutoff energy of 400 eV are used. Both the lattice constants and positions of all atoms are relaxed until the force is less than 0.01 eV/Å. The criterion for the total energy is set as 1×10^{-5} eV. A primitive cell containing 10 atoms and a Monkhorst-Pack k-point mesh of $7 \times 7 \times 7$ are employed. To explore the doping effect, we use a supercell containing 40 atoms with a k-point mesh of $5 \times 5 \times 5$. In the supercell, one of the eight divalent alkaline earth metal atoms A is substituted by a trivalent La or monovalent K atom, which corresponds to a doping concentration of 12.5%. Such a doping technique is commonly applied in double perovskite and DMS systems [18,19,29,30]. To count the electron correlation effects of d orbitals and obtain accurate electronic and magnetic properties, we further apply the screened hybrid HSE06 functional [31,32], which includes the accurate Fock exchange and usually performs much better than the GGA and GGA+U methods [33–35]. To save time, a k-point mesh of $5 \times 5 \times 5$ and $3 \times 3 \times 3$ is used for the primitive cell and doped supercell, respectively. Test calculations including the spin-orbital coupling (SOC) effects are also performed, and we find little change in the band structures of A_2CrMO_6, but a small orbital moment is induced at the Os atom site. The magnetic ordering temperatures of A_2CrMO_6 are estimated by Monte Carlo (MC) simulations with a $12 \times 12 \times 12$ supercell based on the classical Heisenberg Hamiltonian [36].

Double perovskites have found their great success in the development of the concept of half metals [37,38]. The simple crystal structure and potentially very large number of members make double perovskites fertile soils for exploring various spintronic materials. Here, we show how to design AAFMSs with different spin polarization at VBM and CBM by tuning the relative d orbital energy positions of two different transition-metal ions $M1$ and $M2$ in the double perovskite A_2M1M2O_6 (Fig. 1). According to crystal field theory with octahedral symmetry, the d orbitals are split into t_{2g} and e_g orbitals. Further counting the onsite Coulomb interaction, each orbital is again split into spin-up and spin-down orbitals. The former is referred to as crystal field splitting Δ_f and the latter as spin exchange splitting Δ_s. As an example, we here consider the $M1$ ion with three electrons filled in the spin-up $t_{2g\uparrow}$ orbital, while the $M2$ ion with three electrons filled in the spin-down $t_{2g\downarrow}$ orbital, i.e. they are antiferromagnetically coupled, which is permitted by the Goodenough-Kanamori rules [39–41]. In addition, $M1$ is assumed to possess a small spin exchange splitting with respect to crystal field splitting ($\Delta_s < \Delta_f$), while $M2$ has a much larger spin exchange splitting than crystal field splitting ($\Delta_s > \Delta_f$; Fig. 1), which can be easily realized by choosing $M1$ and $M2$ to be $4d/5d$ and $3d$ transition metals, respectively. When the empty spin-down $t_{2g\downarrow}$ orbital of the $M1$ ion lies in the crystal field splitting gap of the $M2$ ion, a HSC is formed where VBM and CBM are fully spin polarized in the same direction [Fig. 1(a)]; when the occupied spin-up $t_{2g\uparrow}$ orbital of the $M1$ ion locates in the crystal field splitting gap of the $M2$ ion, we obtain a BMS with VBM and CBM approaching the Fermi level through opposite spin channels [Fig. 1(b)]. Here, one can see that the spin polarization at VBM and CBM in these AAFMSs is determined by the interplay of crystal field splitting, spin exchange splitting, and d orbital energy location.

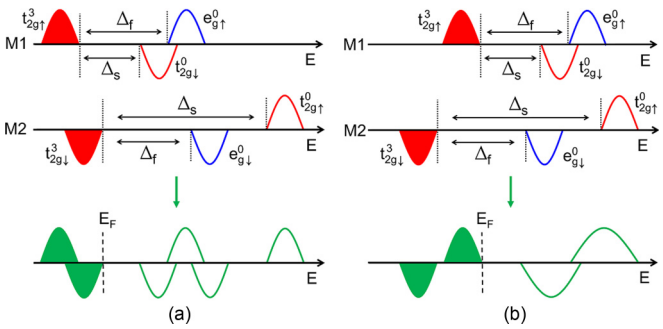

FIG. 1. (Color online) A schematic plot of d orbital mismatch between two different transition metal ions $M1$ and $M2$ in the formation of AFM (a) HSCs and (b) BMSs. Δ_f and Δ_s indicate the size of crystal field splitting and spin exchange splitting, respectively.

Guided by the above design, we take the $M1$ ion to be Ru^{5+}/Os^{5+}, the $M2$ ion to be Cr^{3+}, and the A atom to be divalent alkaline earth metal Ca/Sr/Ba for maintaining charge neutrality, respectively. Among these compounds, Sr_2CrOsO_6 has been synthesized in experiment [8], and we expect others can also be routinely synthesized by solid-state reactions under similar conditions. Considering that Sr_2CrOsO_6 possesses a rhombohedral structure at low and room temperatures, while it becomes cubic above 500 K [8], we calculate both rhombohedral and cubic structures for all A_2CrMO_6 (A = Ca,Sr,Ba; M = Ru,Os). The energy differences between the two phases are summarized in Table I. It can be seen that, while Ba_2CrMO_6 take the cubic form, Sr_2CrRuO_6 slightly prefers rhombohedral structure with similar phase energy difference as Sr_2CrOsO_6, and when evolved to Ca_2CrMO_6, rhombohedral distortion is much more favored, as indicated by much larger energy differences than Sr_2CrOsO_6. Since Sr_2CrOsO_6 has been verified experimentally to be rhombohedral below a relatively high temperature of 500 K, we thus can infer that Ca_2CrMO_6 and Sr_2CrRuO_6 are all likely to keep their rhombohedral structure at room temperature. Here, the optimized lattice parameters of Sr_2CrOsO_6 are very close to the experiment values (0.4% mismatch), demonstrating the accuracy of our calculations.

To investigate the magnetic ground state of the A_2CrMO_6 structures, we perform calculations for two different magnetic configurations, i.e. FM coupling and AFM coupling. The results show that all A_2CrMO_6 structures prefer an AFM order, with the FM state much less stable by an energy difference ΔE_m of about 0.3 eV per chemical formula (Table I). The Néel temperature T_N is further estimated by employing the MC simulations based on the classical Heisenberg Hamiltonian [36]

$$H = -\sum_{i,j} J_{ij} \boldsymbol{S_i} \cdot \boldsymbol{S_j}, \quad (1)$$

TABLE I. Energy difference per chemical formula (ΔE_p) between cubic and rhombohedral phases, space group, lattice parameters (a,α), energy difference per chemical formula (ΔE_m) between FM and AFM states, Néel temperature T_N, spin flip gaps ($\Delta 1, \Delta 2$) for the stable phase.

	ΔE_p (eV)	Space group	a (Å)	α (°)	ΔE_m(eV)	T_N (K)	$\Delta 1$ (eV)	$\Delta 2$ (eV)
Ca_2CrRuO_6	0.715	R-3	5.385	61.059	0.259	355	0.308	1.422
Sr_2CrRuO_6	0.042	R-3	5.521	60.394	0.333	456	0.220	1.147
Ba_2CrRuO_6	[a]	Fm-3m	5.671	60.000	0.351	490	0.066	0.896
Ca_2CrOsO_6	0.726	R-3	5.402	61.114	0.257	355	0.619	1.734
Sr_2CrOsO_6	0.047	R-3	5.538	60.412	0.348	473	0.728	1.434
Ba_2CrOsO_6	[a]	Fm-3m	5.686	60.000	0.384	524	0.848	1.163

[a]An initial rhombohedral cell is automatically optimized to a cubic cell.

where $J = -\Delta E_m/12S^2$ is the nearest $Ru^{5+}/Os^{5+} - Cr^{3+}$ exchange parameter, $S = 3/2$ is the spin of $Ru^{5+}/Os^{5+}/Cr^{3+}$ ion. Here, we only consider the nearest-neighbor exchange interaction, since the next-nearest-neighbor exchange parameter is evaluated to be about one order of magnitude smaller. Later, we will see that this simplified model is sufficient enough to give a reasonable estimate of Néel temperature compared with the experimental one. To obtain T_N, the specific heat $C_V = (\langle E^2\rangle - \langle E^2\rangle)/T^2$ is calculated at first after the system reaches equilibrium at a given temperature. Then T_N is gained by locating the peak position in the $C_V(T)$ plot. The simulated $C_V(T)$ curves are shown in Fig. 2 and the obtained T_N are summarized in Table I. It can be seen that all the magnetic ordering temperatures of A_2CrMO_6 are well above room temperature, with Ba_2CrMO_6 possessing the highest $T_N \sim 500$ K. This is the result of strong Ru^{5+}/Os^{5+}–Cr^{3+} super-exchange interaction. Note that the estimated T_N of rhombohedral Sr_2CrOsO_6 is 473 K, while the experimental measurement is 725 K [8]. This discrepancy is mainly due to the fact that Sr_2CrOsO_6 undergoes a rhombohedral-to-cubic phase transition around 500 K. Thus, we also calculate the Néel temperature of cubic Sr_2CrOsO_6 and find it to be 625 K [Fig. 2(b)]. Considering the tendency to underestimate Néel temperature due to the usage of classical spins in the model [36], this value (625 K) is in reasonable agreement with the experimental one, confirming the validity of our MC simulations. Above all, the A_2CrMO_6 structures are expected to be magnetically ordered at room temperature.

To study the electronic structures of A_2CrMO_6, the DOS are calculated, as shown in Fig. 3. We also examine the DOS of Ca_2CrMO_6 and Sr_2CrMO_6 in their metastable cubic phase, and the results are quite similar. For A_2CrRuO_6, VBM and CBM are fully spin polarized in the spin-down channel, i.e. they are HSCs. Half semiconductors can generate purely spin-polarized electrons and holes upon thermal or optical excitation or simply by applying a gate voltage. Half semiconductors can be characterized by two energy gaps; that is, the spin flip gap in valence band (VB) and conduction band (CB), indicated as $\Delta 1$, $\Delta 2$ in Fig. 3(a). For practical applications, big spin flip gaps are preferred. The values of $\Delta 1$ and $\Delta 2$ for A_2CrRuO_6 are summarized in Table I, from which one can see Ca_2CrRuO_6 is the best HSC among the series. When Ru is replaced by Os, we obtain a BMS, in which the VBM state is fully spin polarized in the spin-up channel, while the CBM state is fully spin polarized in the opposite spin-down channel [Fig. 3(b)]. Such a unique electronic structure enables a feasible approach to manipulate carriers' spin-polarization direction simply by applying a gate voltage. The carrier can be either spin-up or spin-down polarized when the Fermi level crosses the VBM or CBM, which can be controlled by altering the sign of the gate voltage. Similar to HSC, BMS can also be described by two energy gaps $\Delta 1$ and $\Delta 2$, as indicated in Fig. 3(b). All the BMSs present large spin flip gaps of $\sim$1 eV (Table I). Note that a previous theoretical study predicted Sr_2CrOsO_6 to be a zero-gap half semimetallic antiferromagnet [42], which is however inconsistent with the insulating behavior observed in experiment. Their conclusions are based on the local spin-density approximation (LSDA) functional, which is insufficient for such a strongly correlated system [43].

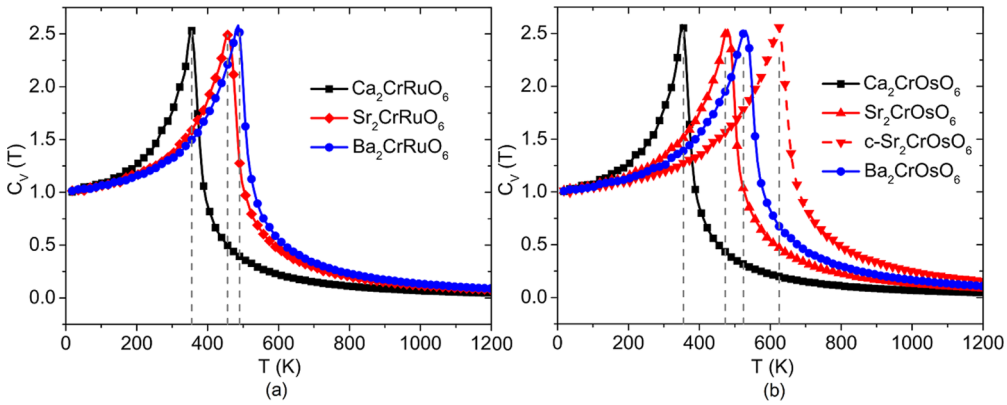

FIG. 2. (Color online) Simulated specific heat C_V with respect to temperature for (a) A_2CrRuO_6 and (b) A_2CrOsO_6 (A = Ca,Sr,Ba). The $C_V(T)$ curve for cubic Sr_2CrOsO_6 (indicated as c-Sr_2CrOsO_6) is also given.

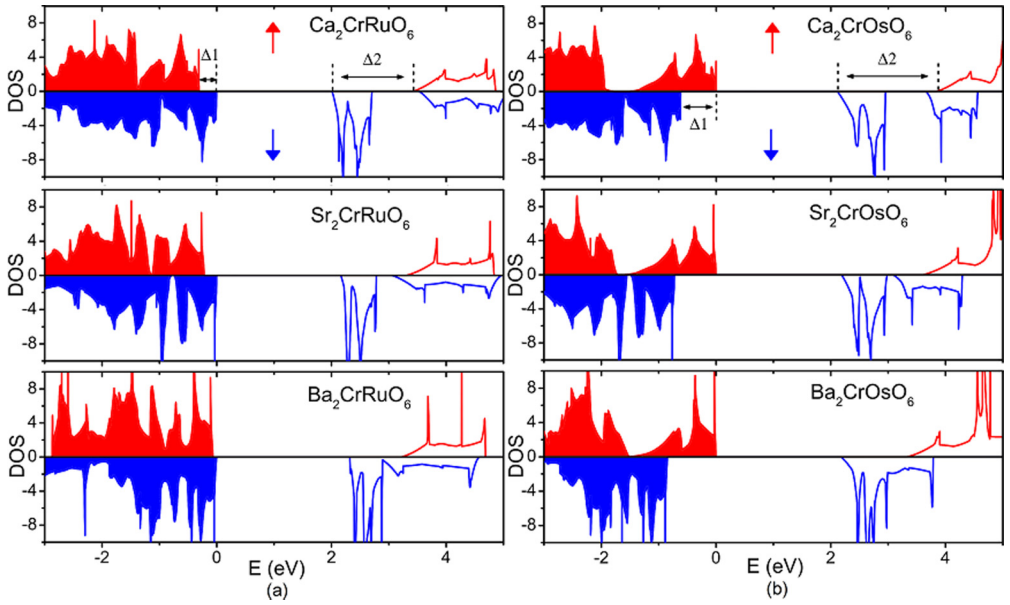

FIG. 3. (Color online) Calculated total DOS for (a) A_2CrRuO_6 and (b) A_2CrOsO_6 (A = Ca,Sr,Ba). Fermi levels are all set to zero.

To further understand the electronic structures of A_2CrMO_6, we plot the atom and orbital projected DOS (PDOS) for Ba_2CrRuO_6 and Ba_2CrOsO_6, respectively. In Ba_2CrRuO_6, the spin-down VBM is mainly contributed by O and Cr atoms, while the spin-down CBM is mostly constructed from O and Ru atom states [Fig. 4(a)]. The analysis of orbital PDOS [Fig. 4(c)] indicates that it is the Cr$t_{2g\downarrow}$ and Ru$t_{2g\downarrow}$ orbitals that contribute to the VBM and CBM, respectively. The empty Ru$t_{2g\downarrow}$ orbital lies in the crystal field splitting gap of the Cr ion, inducing a HSC character, which corresponds to the case in Fig. 1(a). Note that the occupied Ru$t_{2g\uparrow}$ orbital is only slightly lower in energy than the Cr$t_{2g\downarrow}$ orbital, leading to a small spin flip gap in VB. For Ba_2CrOsO_6, the energy of the Os$t_{2g\uparrow}$ orbital increases significantly compared to that of Ru. As a result, it falls into the crystal field splitting gap of the Cr ion, forming a BMS character [Figs. 4(b) and 4(d)], just as the case in Fig. 1(b).

It is generally considered that intrinsic semiconductors are not very useful since they are neither very good insulators nor very good conductors. For practical applications, intrinsic semiconductors are usually doped by heterovalent atoms to significantly increase their free carrier concentration, and their (semi-)conductivity. This is particularly important for medium and wide band gap semiconductors, since their native charge carriers generated by thermal excitation are scarce even at room temperature. Thus, for A_2CrMO_6 with a band gap of about 2 eV, it is a key issue to explore the doping effect. As an example, through partial substitution of Ba with La or K elements, we succeed in obtaining an n- or p-type Ba_2CrMO_6 (M = Ru,Os). As can be seen from Figs. 5(a)

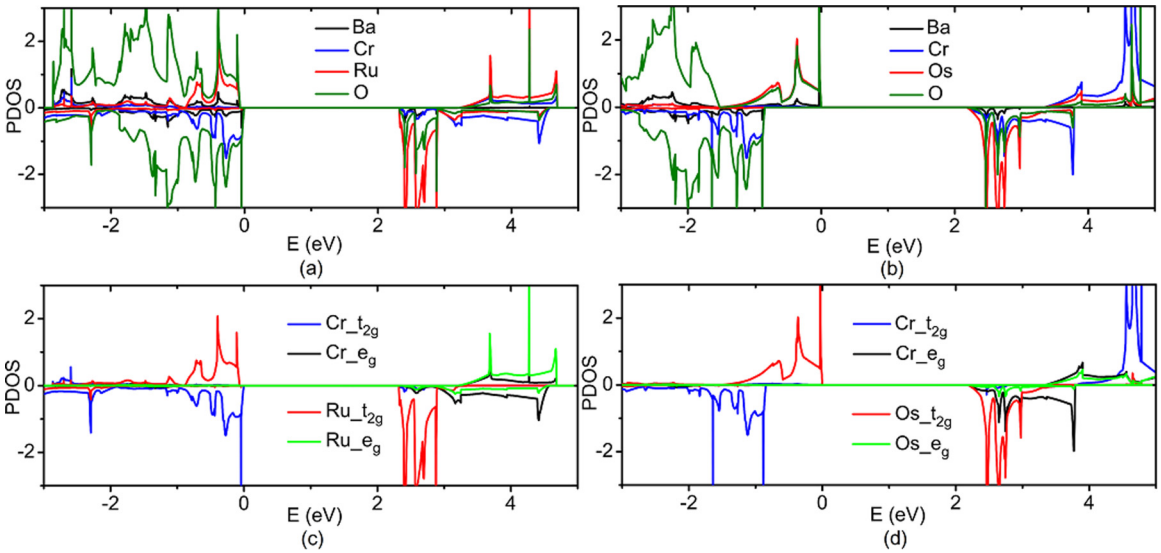

FIG. 4. (Color online) Atom-PDOS for (a) Ba_2CrRuO_6 and (b) Ba_2CrOsO_6. For clarity, the PDOS of oxygen atoms are scaled by a factor of 1/2. Orbital-PDOS for (c) Cr^{3+} and Ru^{5+} ions in Ba_2CrRuO_6 and (d) Cr^{3+} and Os^{5+} ions in Ba_2CrOsO_6. Fermi levels are all set to zero.

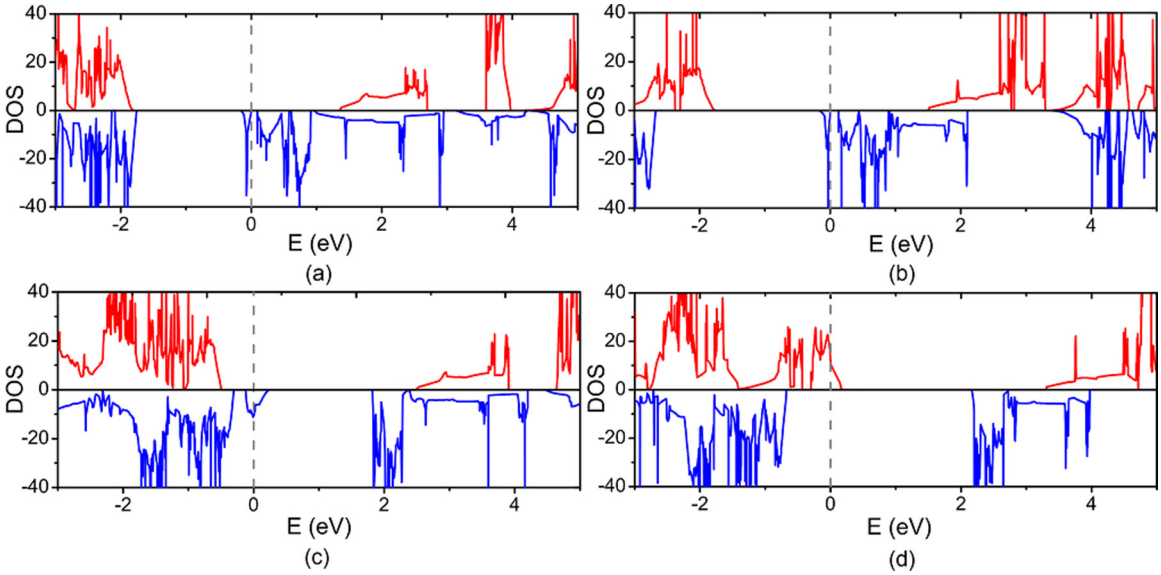

FIG. 5. (Color online) Total DOS for n-type (a) Ba_2CrRuO_6:La and (b) Ba_2CrOsO_6:La and p-type (c) Ba_2CrRuO_6:K and (d) Ba_2CrOsO_6:K. Fermi levels are all set to zero.

and 5(b), under La doping, an occupied donor level emerges just below CB with a displacement around 0.1 eV, which can readily induce n-type conductivity by thermal excitation at room temperature; while under K doping [Figs. 5(c) and 5(d)], the Fermi level crosses the top of VB (note the VB is resplit due to symmetry reduction caused by doping), directly resulting p-type conductivity. Furthermore, another two important features are found. One is the doped system acquires a net spin magnetic moment of 1 μ_B per dopant. The other is that, at room temperature, the free charge carriers in the doped system are expected to be fully spin polarized, owing to the fully spin polarized VBM and CBM, as well as the dopant levels. Thus, we can conclude that chemical doping of AAFMSs can simultaneously generate free carriers, a net spin magnetic moment, and a high spin polarization at the Fermi level.

Ideally, in the doped AAFMSs, the spin polarization is 100% at the Fermi level; while in a real sample, due to the existence of unintended defects, the degree of spin polarization can be reduced. Thus, control of defect formation during the synthesis process would be required, and to meet typical needs of applications, one should ensure a spin polarization above 85%, which is the typical value in DMSs [2,3].

Asymmetric AFM semiconductors provide a way of thinking about magnetic semiconductors and a general scheme for obtaining simultaneous room-temperature magnetic ordering and large spin polarization in a single semiconductor. In the design process, there are two points that should be kept in mind. First, to ensure a semiconducting band structure, partial occupation of spin-orbitals $t_{2g,\sigma}$ and $e_{g,\sigma}(\sigma = \uparrow,\downarrow)$ should be avoided. Nevertheless, in some cases, Jahn-Teller distortion can induce a metal-insulator transition. Second, the Goodenough-Kanamori rules can be used to identify and exclude cases where only FM super-exchange occurs.

Although the design here is merely based on double perovskites which have been well understood and intensively studied by researchers, the concept of AAFMSs is not restricted to double perovskites. All prototype systems that contain multiple magnetic sublattices are possible for the achievement of AAFMSs [44]. Such a possibility will be the focus of future papers.

For AAFMSs, the macroscopic magnetization is either zero (for intrinsic ones) or relatively low (for doped ones) due to AFM coupling of magnetic moments; thus, they may not be applicable in traditional giant magnetoresistance- (GMR) based devices, while the DOS of VBM and CBM are highly spin polarized, endowing these materials great potential of applications in spin-polarized carrier generation, injection, and manipulation.

It is necessary to point out that zero magnetic moment only exists in an ideal case without SOC. After considering SOC, a small net magnetic moment may arise, such as in Sr_2CrOsO_6, but the two characters of room-temperature magnetic ordering and large spin polarization remain [8,9,42,45]. In these situations, the more accurate terminology should be ferrimagnetic semiconductors rather than AFM semiconductors. Actually, it is not essential to demand two transition-metal ions with equal magnetic moments. In a more general picture, using transition-metal ions with different magnetic moments that are ferrimagnetically coupled with each other is also viable to get room-temperature magnetic semiconductors, such as the already known spinel ferrites [46,47].

When one spin channel of AAFMSs closes its band gap, we obtain half metallic antiferromagnets [48], which have been largely explored in various systems due to their versatile applications in electronics and spintronics [49]. Half metallic antiferromagnets provide a platform to get AAFMSs. We envision that half metallic antiferromagnets may be transformed into AAFMSs by lattice distortion, chemical or physical doping, or just changing the transition-metal pairs.

In conclusion, we have proposed a concept of AAFMSs which serves as a general scheme for achieving magnetic

semiconductors with both room-temperature magnetic ordering and large spin polarization. The proposed scheme is confirmed by first-principles design in double perovskite structures A_2CrMO_6 (A = Ca,Sr,Ba; M = Ru,Os). As a type of magnetic semiconductor, current applications of magnetic semiconductors can be directly extended to these materials. By exploiting the mature semiconductor technology, AAFMSs are expected to speed up the realization of spintronic devices that work at room temperature in the near future.

This paper is financially supported by the National Key Basic Research Program (Grant No. 2011CB921404), by the National Natural Science Foundation of China (NSFC) (Grants No. 21421063, No. 91021004, and No. 21233007), by the Chinese Academy of Sciences (CAS) (Grant No. XDB01020300). We used computational resources of Supercomputing Center of University of Science and Technology of China, Supercomputing Center of Chinese Academy of Sciences, Tianjin and Shanghai Supercomputer Centers.

[1] F. Cervantes-Sodi, G. Csányi, S. Piscanec, and A. C. Ferrari, Phys. Rev. B **77**, 165427 (2008).
[2] J. W. Yoo, C.-Y. Chen, H. W. Jang, C. W. Bark, V. N. Prigodin, C. B. Eom, and A. J. Epstein, Nature Mater. **9**, 638 (2010).
[3] X. L. Wang, Phys. Rev. Lett. **100**, 156404 (2008).
[4] S. Ouardi, G. H. Fecher, C. Felser, and J. Kübler, Phys. Rev. Lett. **110**, 100401 (2013).
[5] X. X. Li, X. J. Wu, Z. Y. Li, J. L. Yang, and J. G. Hou, Nanoscale **4**, 5680 (2012).
[6] X. X. Li and J. L. Yang, Phys. Chem. Chem. Phys. **15**, 15793 (2013).
[7] D. Kennedy and C. Norman, Science **309**, 75 (2005).
[8] Y. Krockenberger, K. Mogare, M. Reehuis, M. Tovar, M. Jansen, G. Vaitheeswaran, V. Kanchana, F. Bultmark, A. Delin, F. Wilhelm, A. Rogalev, A. Winkler, and L. Alff, Phys. Rev. B **75**, 020404(R) (2007).
[9] H. L. Feng, M. Arai, Y. Matsushita, Y. Tsujimoto, Y. Guo, C. I. Sathish, X. Wang, Y. H. Yuan, M. Tanaka, and K. Yamaura, J. Am. Chem. Soc. **136**, 3326 (2014).
[10] T. Kimura, S. Kawamoto, I. Yamada, M. Azuma, M. Takano, and Y. Tokura, Phys. Rev. B **67**, 180401(R) (2003).
[11] M. Azuma, K. Takata, T. Saito, S. Ishiwata, Y. Shimakawa, and M. Takano, J. Am. Chem. Soc. **127**, 8889 (2005).
[12] N. S. Rogado, J. Li, A. W. Sleight, and M. A. Subramanian, Adv. Mater. **17**, 2225 (2005).
[13] Y. Singh, M. A. Green, Q. Huang, A. Kreyssig, R. J. McQueeney, D. C. Johnston, and A. I. Goldman, Phys. Rev. B **80**, 100403(R) (2009).
[14] P. Wadley, V. Novák, R. P. Campion, C. Rinaldi, X. Martí, H. Reichlová, J. Železný, J. Gazquez, M. A. Roldan, M. Varela, D. Khalyavin, S. Langridge, D. Kriegner, F. Máca, J. Mašek, R. Bertacco, V. Holý, A. W. Rushforth, K. W. Edmonds, B. L. Gallagher, C. T. Foxon, J. Wunderlich, and T. Jungwirth, Nat. Commun. **4**, 2322 (2013).
[15] H. Ohno, A. Shen, F. Matsukura, A. Oiwa, A. Endo, S. Katsumoto, and Y. Iye, Appl. Phys. Lett. **69**, 363 (1996).
[16] A. H. MacDonald, P. Schiffer, and N. Samarth, Nature Mater. **4**, 195 (2005).
[17] Z. Deng, C. Q. Jin, Q. Q. Liu, X. C. Wang, J. L. Zhu, S. M. Feng, L. C. Chen, R. C. Yu, C. Arguello, T. Goko, F. Ning, J. Zhang, Y. Wang, A. A. Aczel, T. Munsie, T. J. Williams, G. M. Luke, T. Kakeshita, S. Uchida, W. Higemoto, T. U. Ito, B. Gu, S. Maekawa, G. D. Morris, and Y. J. Uemura, Nat. Commun. **2**, 422 (2011).
[18] K. Zhao, Z. Deng, X. C. Wang, W. Han, J. L. Zhu, X. Li, Q. Q. Liu, R. C. Yu, T. Goko, B. Frandsen, L. Liu, F. Ning, Y. J. Uemura, H. Dabkowska, G. M. Luke, H. Luetkens, E. Morenzoni, S. R. Dunsiger, A. Senyshyn, P. Böni, and C. Q. Jin, Nat. Commun. **4**, 1442 (2013).
[19] C. Ding, H. Man, C. Qin, J. Lu, Y. Sun, Q. Wang, B. Yu, C. Feng, T. Goko, C. J. Arguello, L. Liu, B. A. Frandsen, Y. J. Uemura, H. Wang, H. Luetkens, E. Morenzoni, W. Han, C. Q. Jin, T. Munsie, T. J. Williams, R. M. D'Ortenzio, T. Medina, G. M. Luke, T. Imai, and F. L. Ning, Phys. Rev. B **88**, 041102(R) (2013).
[20] T. Dietl, H. Ohno, F. Matsukura, J. Cibert, and D. Ferrand, Science **287**, 1019 (2000).
[21] T. Dietl, Nature Mater. **9**, 965 (2010).
[22] A. Bonanni and T. Dietl, Chem. Soc. Rev. **39**, 528 (2010).
[23] T. Dietl and H. Ohno, Rev. Mod. Phys. **86**, 187 (2014).
[24] X. Li, X. Wu, and J. Yang, J. Mater. Chem. C **1**, 7197 (2013).
[25] X. Li, X. Wu, and J. Yang, J. Am. Chem. Soc. **136**, 11065 (2014).
[26] J. P. Perdew, K. Burke, and M. Ernzerhof, Phys. Rev. Lett. **77**, 3865 (1996).
[27] G. Kresse and J. Furthmüller, Phys. Rev. B **54**, 11169 (1996).
[28] P. E. Blöchl, Phys. Rev. B **50**, 17953 (1994).
[29] J. Navarro, C. Frontera, Ll. Balcells, B. Martínez, and J. Fontcuberta, Phys. Rev. B **64**, 092411 (2001).
[30] J. B. Philipp, P. Majewski, L. Alff, A. Erb, R. Gross, T. Graf, M. S. Brandt, J. Simon, T. Walther, W. Mader, D. Topwal, and D. D. Sarma, Phys. Rev. B **68**, 144431 (2003).
[31] J. Heyd, G. E. Scuseria, and M. Ernzerhof, J. Chem. Phys. **118**, 8207 (2003).
[32] J. Heyd, G. E. Scuseria, and M. Ernzerhof, J. Chem. Phys. **124**, 219906 (2006).
[33] M. Marsman, J. Paier, A. Stroppa, and G. Kresse, J. Phys.: Condens. Mater. **20**, 064201 (2008).
[34] J. L. F. Da Silva, M. V. Ganduglia-Pirovano, J. Sauer, V. Bayer, and G. Kresse, Phys. Rev. B **75**, 045121 (2007).
[35] X. D. Wen, R. L. Martin, L. E. Roy, G. E. Scuseria, S. P. Rudin, E. R. Batista, T. M. McCleskey, B. L. Scott, E. Bauer, J. J. Joyce, and T. Durakiewicz, J. Chem. Phys. **137**, 154707 (2012).
[36] H. J. Xiang, S.-H. Wei, and M.-H. Whangbo, Phys. Rev. Lett. **100**, 167207 (2008).
[37] K.-I. Kobayashi, T. Kimura, H. Sawada, K. Terakura, and Y. Tokura, Nature **395**, 677 (1998).
[38] W. E. Pickett, Phys. Rev. B **57**, 10613 (1998).

[39] J. B. Goodenough, Phys. Rev. **100**, 564 (1955).
[40] J. B. Goodenough, J. Phys. Chem. Solids **6**, 287 (1958).
[41] J. Kanamori, J. Phys. Chem. Solids **10**, 87 (1959).
[42] K. W. Lee and W. E. Pickett, Phys. Rev. B **77**, 115101 (2008).
[43] O. N. Meetei, O. Erten, M. Randeria, N. Trivedi, and P. Woodward, Phys. Rev. Lett. **110**, 087203 (2013).
[44] K. Özdoğan, E. Şaşıoğlu, and I. Galanakis, J. Appl. Phys. **113**, 193903 (2013).
[45] H. Wang, S. Zhu, X. Ou, and H. Wu, Phys. Rev. B **90**, 054406 (2014).
[46] Z. Szotek, W. M. Temmerman, D. Ködderitzsch, A. Svane, L. Petit, and H. Winter, Phys. Rev. B **74**, 174431 (2006).
[47] J.-B. Moussy, J. Phys. D: Appl. Phys. **46**, 143001 (2013).
[48] H. van Leuken and R. A. de Groot, Phys. Rev. Lett. **74**, 1171 (1995).
[49] X. Hu, Adv. Mater. **24**, 294 (2012).